The Influence of the Singularity-Enhanced Density of States on the Isotope Effect in a Bond Asymmetric Model for Cu-O Based High-T_C Superconductor

Seiichi SEKI

The Influence of the Singularity-Enhanced Density of States on the Isotope Effect in a Bond Asymmetric Model for Cu-O Based High-T_C Superconductor

Seiichi SEKI

Abstract

In the presence of an asymmetry with respect to the x- and y-directions, possible singularities in the electronic density of states are investigated in the Cu-O 2D plane model. The mixing of the Cu- and O- hole states leads to an interesting behavior of the density of states, which induces the drastic reduction of the isotope effect.

§ 1. Introduction

The discovery of high-T_C superconductivity in Cu-based oxide superconductors has attracted strong interest in possible new mechanisms for the phenomena. To account for the origin of superconductivity in these materials, many authors have proposed various mechanisms.[1)-5)] However, the problem may still be controversial at the present time.

In the $YBa_2Cu_3O_{7-x}$ compounds, two dimensihnal Cu(2)-O(a, b) layers are considered to be relevant to the conduction process. In fact, the interlayer transfer integral is two orders of magnitude smaller than the intralayer transfer. At low temperatures, these layers show a certain type of asymmetry with respect to the x- and y-directions, i.e. formation of an oblique lattice, where the distance between neighboring Cu(2) and O(a) atoms is slightly longer than that between Cu(2) and O(b) atoms.[6)] In such an

asymmetric situation, the Coulomb potential energies at O(a) and O(b) sites would be different from each other, together with the anisotropy of the intralayer transfer integal. When the temperature exceeds a certain critical value, the oblique lattice changes into the square one. The high-T_C superconductivity is not observed in this symmetric structure. Such an experimental evidence suggests that the structural asymmetry (bond asymmetry) may play a significant role in realizing the high-T_C state.[7]

For the copper and oxgen ions in the Cu^{++} and O^{--} states, the hole numbers on these ions are respectively given by 1 and 0. The additional holes to such an ionic state would then go mainly into the O-levels to avoid the strong Coulomb repulsion at Cu-sites. Thus, the charge carriers of superconductivity are considered mainly on the oxgen atoms. This fact enables us to introduce the O-hole dominant model,[7,8] where the available Cu-states are eliminated by standard perturbation theory, and only the O-sublattice is taken into account. In this O-hole dominant model, the potential energy difference between the O(a) and O(b) states induces the splitting of the O-band into two subbands. The upper (lower) edge of the lower (upper) subband shows the singularity described by the expression, $E^{-1/2}\log E$, $(E\rightarrow 0+)$, when the O-hole hopping occurs only between nearest-neighbor O-sites. Furthermore, the extremely small but nonvanishing interlayer transfer changes the above singularity into the two singularities specified by $(\log E)^2$ and $\log E$ with with $E\rightarrow 0+$, which are located very closely to each other; the distance betwen them is of the order of the interlayer transfer integral. As shown in the preceding paper (I),[8] such a singularity-enhanced density of tates induces an interesting chemical potential dependence of the isotope effect. In particular, the isotope effect is drastically reduced when the chemical potential comes close to these singularities.

The O-hole dominant model described above is valid for the

large limit of the Coulomb repulsion at Cu-sites. In the compounds we are considering, the Coulomb repulsions at Cu- and O-sites are respectively estimated to be U_d=5–8eV and U_o=2–3eV, and the Coulomb repulsion V between neighboring Cu- and O-holes is $V \lesssim$ leV. Such an estimate suggests that the contribution of the Cu-holes to supercurrents is not necessarily negligible. Thus, in a more refined treatment we are required to consider the Cu- and O-holes, simultaneously, and to investigate the mixing of them. The purpose of this paper is to point out that the appreciable mixing of the Cu- and O-hole states induces somewhat different types of singuiarities and different shape of the density of states from those in the O-hole dominant model presented in the paper I. We also aim at investigating how the singularity-enhanced density of states in the Cu- and O-hole mixing model affects on the isotope effect and the tunneling currents, both of which are sensitive to the density of states.

In the Cu-O based high-T_C superconductors, many physical quantities experimentally observed are averaged over the x- and y-directions. For example, the magnetic penetration depth λ is estimated to be 1000–1500 Å, which is an average over λ_x and λ_y. In order to measure λ_x and λ_y separately, large untwinned crystals are required to be available. The in-plane anisotropy of λ leads to the distortion of triangle lattice of magnetic fluxes, and the observed distortion yields the following effective mass anisotropy, m_y/m_x=1.2–1.4[9,10] (λ is proportional to $m^{1/2}$). This result also suggests that the analysis of the in-plane anisotropy is necessary. In some respect the following discussion will contribute to clarifying the effect of the in-plane anisotropy, although the model employed is a simple one.

§ 2. Single particle eigənstates

We cousider a single plane model described by the following Hamiltonian,

$$H=H_0+H_C \tag{2.1}$$

where the one-particle and Coulom repulsion terms, H_0 and H_C, are respectively given by

$$H_0=E_d\sum_{is}d_{is}^+d_{is}+E_a\sum_{ms}a_{ms}^+a_{ms}+E_b\sum_{ns}b_{ns}^+b_{ns}$$
$$+t_a/2\sum_{\langle im\rangle s}(d_{is}^+a_{ms}+h.\,c.)+t_b/2\sum_{\langle in\rangle s}(d_{is}^+b_{ns}+h.\,c.) \tag{2.2}$$

and

$$H_{int}=U_d/2\sum_{is}n_{is}^dn_{i-s}^d+U_0/2\sum_{ms}n_{m-s}^a$$
$$+U_0/2\sum_{ns}n_{ns}^bn_{n-s}^b+V\sum_{\langle im\rangle}\sum_{s_1s_2}n_{is_1}^dn_{ms_2}^a$$
$$+V\sum_{\langle in\rangle}\sum_{s_1s_2}n_{is_1}^dn_{ns_2}^b \tag{2.3}$$

In the above definitions, we have employed a hole picture to simplify the whole discussion. Thus, the operators d_{is}^+, a_{ms}^+ and b_{ns}^+ create s-spin holes at Cu-, O(a)- and O(b)-sites, respectively, and the symbol $\langle\ \rangle$ stands for a pair of nearest-neighbor sites. U_d and U_0 represent the magnitudes of the Coulomb repulsions at Cu- and O(a, b)-sites, and V is derived from the intersite Coulomb repulsion between neighboring Cu- and O-holes. n_{is}^d, n_{ms}^a and n_{ns}^b are the hole number operators at Cu-, O(a) and O(b)-sites, respectively. In the hole picture, we have $E_d<E_a$, E_b.

We begin with considering the single-particle eigenstates of H_0 given by (2.2). Fourier-transforming H_0, we have

$$H_9=E_d\sum_{ks}d_{ks}^+d_{ks}+E_a\sum_{ks}a_{ks}^+a_{ks}+E_b\sum_{ks}b_{ks}^+b_{ks}$$
$$+t_a\sum_{ks}\cos k_x(d_{ks}^+a_{ks}+h.\,c.)+t_b\sum_{ks}\cos k_y(d_{ks}^+b_{ks}+h.\,c.) \tag{2.4}$$

where the x- and y-components of 2D momentum k are confined to the first Brillouin zone, i.e. $-\pi/2\leqq k_x,\ k_y\leqq\pi/2$. The linear transformation

$$\begin{bmatrix}Q_{1s}^+(k)\\Q_{2s}^+(k)\\Q_{3s}^+(k)\end{bmatrix}=U\begin{bmatrix}d_{ks}^+\\a_{ks}^+\\b_{ks}^+\end{bmatrix} \tag{2.5}$$

diagonalizes H_0 as follows

$$H_0=\sum_{j=1-3}\sum_{ks}E_j^0(k)Q_{js}^+(k)Q_{js}(k),\quad (E_1^0<E_2^0<E_3^0) \tag{2.6}$$

with keeping usual anticommutation rules, $[Q_{is}^{+}(k),\ Q_{js}(k')]_{+}=\delta_{ij}\delta_{kk'}$ etc. The eigenenergies $E_j^0(k)$ are obtained from the equation

$$E-E_d=f_k^2/(E-E_a)+g_k^2/(E-E_b) \tag{2.7a}$$

or equivalently

$$\begin{aligned} Z(E.\ k)&=(E-E_d)(E-E_a)(E-E_b)-f_k^2(E-E_b)-g_k^2(E-E_a)\\ &=(E-E_1^0(k))(E-E_2^0(k))(E-E_3^0(k))=0 \end{aligned} \tag{2.7b}$$

with $f_k=t_a\cos k_x$, $g_k=t_b\cos k_y$ and $E=E_j^0(k)$,

The eigenstates with energies $E_1^0(k)$ and $E_3^0(k)$ corresppond to the extended antibonding and bonding Cu-O electronic bands, respectively. Their amplitudes take comparatively large values at Cu-sites, whereas the E_2-holes have large amplitudes at O-sites. When $E_a=E_b$. the E_2-holes are completely localized at O-sites, giving a delta function spike at $E=E_a$ to the density of states. If the small transfer integral between neighboring O(a) and O(b) sites is considered in the Hamiltonian (2.1), the delta function spike changes into a narrow band with finite bandwidth. However, such a change does not yield serious modification of the discussion presented below.

The density of states $D_1(E)$ for the E_1-band is given by

$$D_1(E)=(\pi/2)^{-2}\int_0^{\pi/2}dk_x\int_0^{\pi/2}dk_y\delta(E-E_1^0(k)) \tag{2.8}$$

From (2.7b) it follows that

$$\begin{aligned} \delta(E-E_1^0(k))&=\delta(E-E_1^0(k))(E-E_2^0(k))(E-E_3^0(k))\\ &\times\lim_{E\to E_1^0(k)}|(E-E_2^0(k))(E-E_3^0(k))|\\ &=[\partial Z(E,\ k)/\partial E]_{E=E_1^0(k)}\delta(Z(E,\ k)) \end{aligned} \tag{2.9}$$

Since $E_j^0(k)$ are functions of $\cos^2 k_x$ and $\cos^2 k_y$, it is convenient for later calculations to write as $E_j^0(k)=E_j^0(\cos^2 k_x,\ \cos^2 k_y)=E_j^0(x,\ y)$ with $x=\cos^2 k_x$ and $y=\cos^2 k_y$. Then, combination of (2.8) and (2.9) leads to

$$\begin{aligned} D_1(E)&=\pi^{-2}t_b^{-2}|E-E_a|^{-1}\int_0^1 dx[x(1-x)]^{-1/2}[h(x,E)\\ &\times(1-h(x,E))]^{-1/2}\theta(h(x,E))\theta(1-h(x,E))|3[E_1^0 \end{aligned}$$

$$\times (x, h(x, E))]^2 - 2(E_d + E_a + E_b) E_1^0(x, h(x, E)) + E_d E_a + E_a E_b + E_b E_d - t_a^2 x - t_b^2 h(x, E) | \quad (2.10)$$

with

$$h(x, E) = [(E - E_b)/t_b^2][E - E_a - t_a^2 x/(E - E_a)] \quad (2.11)$$

and the step fuhction

$$\theta(x) = \begin{cases} 1 & \text{for } x > 0 \\ 0 & \text{otherwise} \end{cases} \quad (2.12)$$

After somewhat lengthy calculation, we have from (2.10) logarithmic divergence at the two points (Fig. 1)

$$E = [E_a + E_d - \{(E_a - E_d)^2 + 4t_a^2\}^{1/2}]/2 = E_{p_1} \quad (2.13a)$$

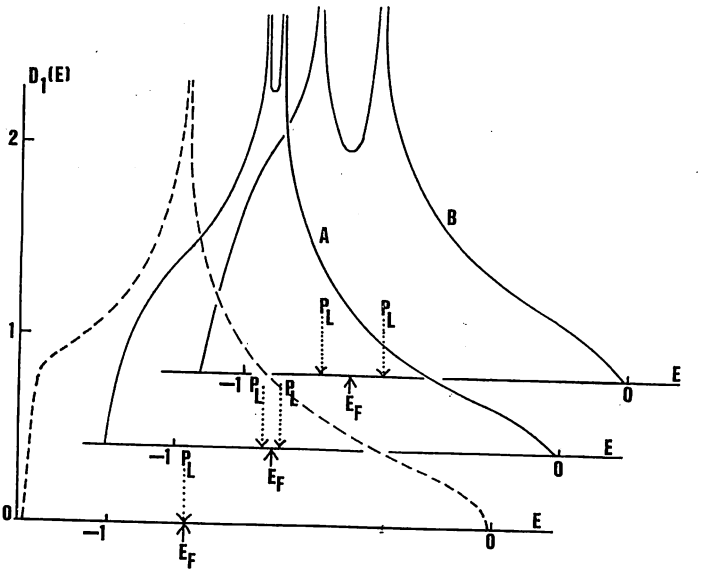

Fig. 1. The density of states for the E_1-band, $D_1(E)$, defined by (2.10), in the absence of the Coulomb repulsion. The solid curves A and B correspond to the parameter values i) $t_a = t_b = 1$ and ii) $t_b = 1.1$, $t = 0.9$ respectively, with $E^d = 0$ and $E_a = E_b - 0.1 = 0.5$. The dashed curve corresponds to the symmetric case ($t_a = t_b = 1$ and $E_a = E_b = 0.5$, $E_d = 0$). P_L means the position of the logarithmic van Hove singularity and E_F the Fermi energy for the half-filled E_1-band.

$$E=[E_b+E_d-\{(E_b-E_d)^2+4t_b^2\}^{1/2}]/2=E_{p_2} \tag{2.13b}$$

Thisdive rgence is equivalent to the two-dimensional van Hove singularity. For the symmetric case, i.e. $E_a=E_b$ and $t_a=t_b$, the logarithmic divergence appears only at $E=E_{p_1}=E_{p_2}$ (the dashed curve in Fig. 1); then for the half-filled E_1-band the Fermi energy is located just at the logarithmic peak. On the other hand, when at least one of the two relatins $E_a\neq E_b$ and $t_a\neq t_b$ is satisfied, two logarithmic peaks appear at different positions (2.13a, b). In this two-peak structure, the Fermi energy is located between the two peaks for the half-filled E_1-band. Thus, when the E_1-band is half-filled, the transition from the symmetric to asymetric state leads to the drastic reduction of the density of states at the Fermi energy for the E_1-band.

In the following discussion, we assume that in the presence of the additional holes, the E_1-band is half-filled in the hole picture. Roughly speaking, this state corresponds to the ionic configuration, Cu^{++} and O^{--}. Then, the Coulomb repulsion terms in (2.3) (particularly, the U_d-term) yield the finite gap between the occupied and unoccupied E_1-energy levels. The unoccupied E_2- and E_3-bands are also modified by the Coulomb repulsion terms. Applying the Hartree-Fock approximation to (2.3), we have the following expressions for the hole dispersions of the unoccupied E_j-levels ($j=1, 2, 3$),

$$E_j(k)=E_j^0(k)+E_{j,\ \mathrm{Coulomb}}(k) \tag{2.14}$$

where $E_j^0(k)$ are defined by (2.6) and $E_{j,\ \mathrm{Coulomb}}(k)$ are given by

$$\begin{aligned}E_{j,\ \mathrm{Coulomb}}(k)=&\sum_{i=1,2,3}U_i|w_{0j}(k)|^2+2[V_{1l}\{|w_{2j}(k)|^2\\&+|w_{3j}(k)|^2\}+(V_{2l}+V_{3l})|w_{1l}(k)|^2\\&-(V_1^x\cos k_x+V_2^x\sin k_x)w_{1j}(k)w_{2j}(k)\\&-(V_1^x\cos k_y+V_2^x\sin k_y)w_{1j}(k)w_{3j}(k)\end{aligned} \tag{2.15}$$

with $w_{ij}(k)$ being the $i-j$ components of the inverse matrix of U defined by (2.5) and

$$U_1=U_d\sum_{k(<k_F)}|w_{11}(k)|^2 \tag{2.16a}$$

$$U_i = U_0 \sum_{k(<k_F)} |w_{i1}(k)|^2 \qquad (i=2,3) \tag{2.16b}$$

$$V_j = V \sum_{k(<k_F)} |w_{j1}(k)|^2 \qquad (i=1,2,3) \tag{2.16c}$$

and

$$V_i^x = V \sum_{k(<k_F)} (\delta_{1i} \cos k_x + \delta_{2i} \sin k_x) w_{21}(k) w_{11}(k) \tag{2.17a}$$

$$V_i^y = V \sum_{k(<k_F)} (\delta_{1i} \cos k_y + \delta_{2i} \sin k_y) w_{31}(k) w_{11}(k)$$

$$(i=1,2) \tag{2.17b}$$

Here δ means Kronecker's delta function. We note that for a set of adequate parameter values, $E_2(k)$ becomes smaller than $E_1(k)$ in a certain range of the first Brillouin zone, as illustrated in Fig. 2. The dashed curve represents the Fermi surface for the half-filled E_1-band, the curve deviating from the symmetric case, i.e. $|k_x|+|k_y|=\pi/2$. Both the hatched and dotted regions are empty for the half-filled case. The relation, $E_2(k)<E_1(k)$, is satisfied in the hatched region, whereas we have $E_1(k)<E_2(k)$ in the dotted region. Thus, after completion of occupying the dotted region, the rest of the additional holes will go into the E_2-hand. The dotted region becomes narrower with increasing U_d, and for sufficietly large U_d the inequality $E_2(k)<E_1(k)$ is satisfied in the whole region of the first Brillouin zone. Then, all the additional holes occupy the E_2-band.

From numerical calculation, we have confirmed that the k-dependence of $E_{j,\ \mathrm{Coulomb}}(k)$ is not so strong compared with that of $E_j^0(k)$; the contours of $E_i(k)$ in the k-space are very similar to those of $E_j^0(k)$. This enables us to introduce the approximation,

$$E_{j,\ \mathrm{Coulomb}}(k) \to \langle E_{j,\ \mathrm{Coulomb}}(k) \rangle_{AV} = E_{j\cdot c} \tag{2.18}$$

where $\langle \ldots \rangle_{AV}$ means taking the average of $E_{j,\ \mathrm{Coulomb}}(k)$ over the first Brillouin zone. Such a simplification leads to the following expression for the density of states for the E_2-band

$$D_2(E) = (\pi/2)^{-2} \int_0^{\pi/2} dk_x \int_0^{\pi/2} dk_y \delta(E - E_2(k))$$

$$= \pi^{-2} t_b^{-2} |\overline{E} - E_a|^{-1} \int_0^1 dx [x(1-x)]^{-1/2} [h(x, \overline{E})(1 - h(x, \overline{E}))]^{-1/2}$$

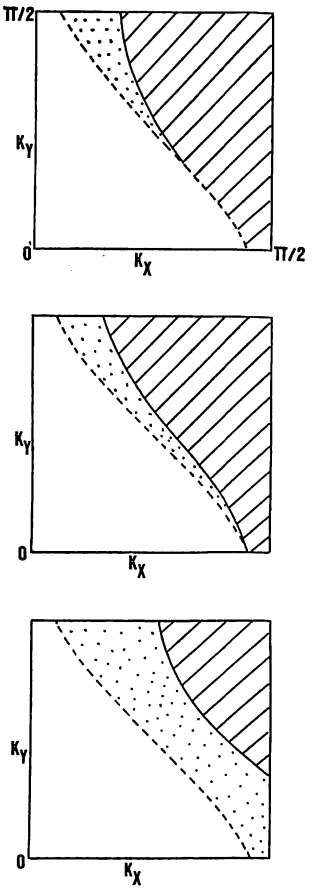

Fig. 2. In the hatched region, the relation $E_2(k)<E_1(k)$ is satisfied in the first Brillouin zone. In the dotted region (where E_1-levels are also unoccupied), $E_1(k)<E_2(k)$. $t_a=t_b$, $E_a=E_b-0.1=0.5$ and (U_d, U_0, V) is given by (a) (6, 2, 0), (b) (6, 2, 1) and (c) (5, 2, 1). The dashed curve represents the Fermi surface for the half-filled E_1-band.

$$\times\theta(h(x,\overline{E}))\theta(1-h(x,\overline{E}))\,|\,3[E_2^0(x,h(x,\overline{E}))]^2-2(E_d+E_a+E_b)$$
$$\times E_2^0(x,h(x,\overline{E}))+E_aE_b+E_bE_a-t_a^2x-t_b^2h(x,\overline{E})\,| \qquad (2.19)$$

with $\overline{E}=E-E_{2,c}$. From the step functions in the above integrand,

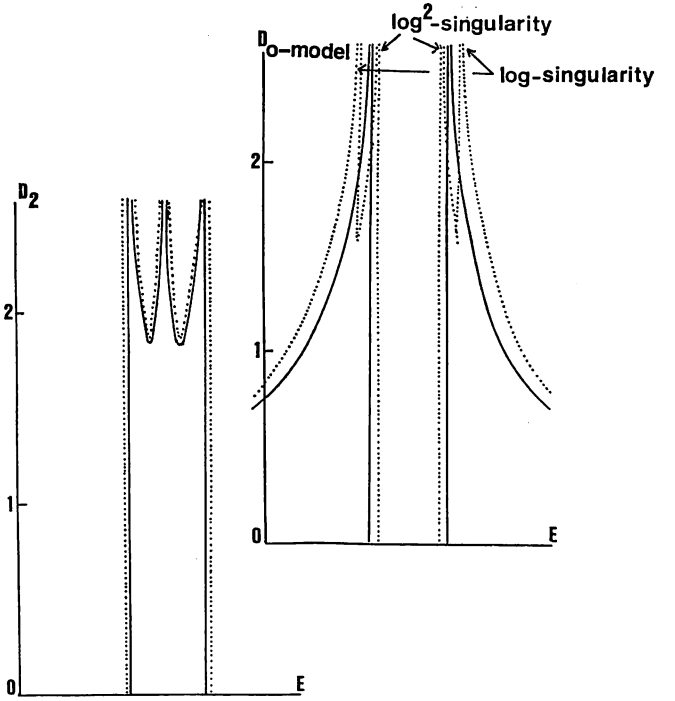

Fig. 3. The solid curves represent the densities of states, D_2 (defined by (2.19)) and $D_{0\text{-model}}$. Here $D_{0\text{-model}}$ is the density of states in the O-hole dominant model. The parameter values are the same as those employed in Fig. 2(a). The dotted curves give the modifications of D_2 and $D_{0\text{-model}}$ due to the small interlayer transfer t_z $(=10^{-2}t_a)$.

it is verified that D_2 is nonzero in the range, $E_a+E_{2,c} \leqq E \leqq E_b+E_{2,c}$. From (2.19), it is verified that

$$D_2(E)=\text{const.}\times(E-E_a-E_{2,c})^{-1/2} \quad E\to E_a+E_{2,c}+0 \tag{2.20a}$$

$$D_2(E)=\text{const.}\times(E_b+E_{2,c}-E)^{-1/2} \quad E\to E_b+E_{2,c}-0 \tag{2.20b}$$

We also confirm from (2.19) that a logarithmic singularity

$$D_2(E)\propto\log|E-E_L-E_{2,c}| \tag{2.21}$$

appears as another peak near the center of the subband, where E_L is determined from

$$E_L - E_a = t_a^2/(E_L - E_a) + t_b^2/(E_L - E_a) \qquad (2.22)$$

with $E_b < E_L < E_b$. In Fig. 3, we present the density of states, $D_2(E)$, which shows the three sharp peaks, i.e. the two peaks (given by (2.20a, b)) at the upper and lower band edges and the peak near the center of the band. As is found in Fig. 3 the shape of $D_2(E)$ is considerably different from the shape of $D_{0\text{-model}}$ (which is the density of states in the O-hole dominant model). The solid curves represent D_2 and $D_{0\text{-medol}}$ in a single layer model, and the dotted curves the modifications due to the small interlayer transfer (refer the next section). One of the characteristic features of $D_{0\text{-model}}$ is the splitting into two subbands; for the solid curves, the band edge peaks are specified by the $E^{-1/2}\log E$-singularity with $E \to 0$, and for the dotted curves the two peaks in each subband are specified by the $(\log E)^2$- and $\log E$-singularities. For the Fermi energy close to theses singularities, comparatively high comcentration of holes ($n_c \sim 0.5$) is required. On the other hand, in the Cu- and O-hole mixing model the concentration n_c of the additional holes to realize the Fermi energy close to the singular point is dependent on the parameter values of U_d, U_0, V and t_a, t_b. For example, for $(U_d, U_0, V) = (6, 2, 1)$ with $t_a = t_b = 1$, we have $n_c \sim 0.1$. When $U_d > 8$ with $(U_0, V) = (2, 1)$ and $t_b = t_b = 1$, all the unoccupied E_1-levels shift to higher energy side than the bottom of the E_2-band. Then the concentration n_c becomes extremely low. In Fig. 4, we present the relative positions of the unoccupied E_1- and E_2-bands.

As described above, consideration of the small interlayer transfer leads to the $(\log E)^2$- and $\log E$-singularities (located very closely to each other) of $D_{0\text{-model}}$. However, the Cu- and O-hole mixing model does not necessarily yield such singularities. In fact, in the presence of the interlayer transfer D_2 does not show any singularity, although its peak structure is almost

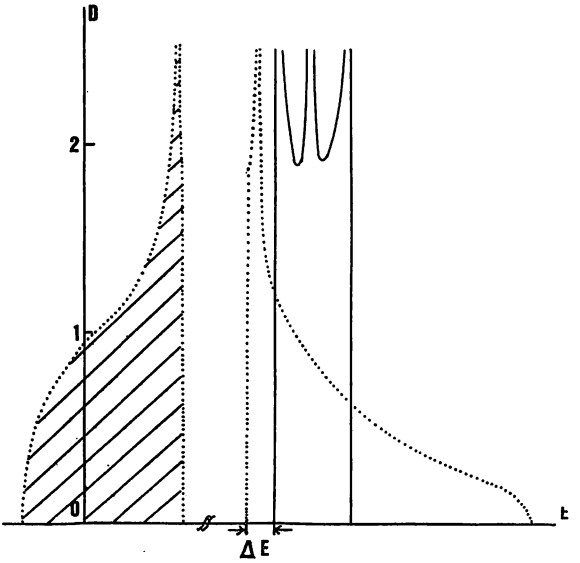

Fig. 4. The occupied and unoccupied E_1-bands (the dotted curves) separated by a finite energy gap (which is resulted from the Coulomb repulsion, mainly at *Cu*-sites). The hatched region is occupied by holes (half-filled). $\triangle E$ is the distance measured from the bottom of the E_2-band. For the parameter values employed in Fig. 2(a), we have $\triangle E=0.03$.

unchanged. To see this, the next section is devoted to a study of the effect of the small interlayer transfer.

§ 3. The effect of the iuterlayer transfer

In this section, we consider the interlayer hopping processes decribed by the Hamiltonian

$$H_{\text{inter}}=\sum_{\langle L_1L_2\rangle}\sum_{mn}\sum_{s}[t^{L_1L_2}_{dd,\,mn}d^{+}_{L_1,\,ms}d_{L_2,\,ns}+t^{L_1L_2}_{aa,\,mn}a^{+}_{L_1,\,ms}a_{L_2,\,ns}$$
$$+t^{L_1L_2}_{bb,\,mn}b^{+}_{L_1,\,ms}b_{L_2,\,ns}+t^{L_1L_2}_{da,\,mn}(d_{L_1,\,ms}a_{L_2,\,ns}+h.\,c.)$$
$$+t^{L_1L_2}_{db,\,mn}(d^{+}_{L_2,\,ms}b_{L_2,\,ns}+h.\,c.)+t^{L_1L_2}_{ab,\,mn}(a^{+}_{L_1,\,ms}b_{L_2,\,ns}+h.\,c.) \tag{3.1}$$

where L_1 and L_2 are layer indices, and $<L_1L_2>$ means taking nearest-neighbor layers. m and n are lattice site indices. Sub-

stituting the following Fourier-transform into (3.1)

$$d_{L,\,ms}=\sum_k \exp(ikR_m)\, d_{L,\,ks},\ \text{et al.}, \tag{3.2}$$

with the linear momentum k within the layer, and making use of (2.5), we obtain

$$H_{\text{inter}}=\sum_{\langle L_1 L_2\rangle}\sum_s\sum_{k_1 k_2} t^{L_1L_2}_{ij,\,k_1k_2} Q^{+}_{L_1,\,is}(k_1)\, Q_{L_2,\,js}(k_2) \tag{3.3}$$

where $t^{L_1L_2}_{ij,\,k_1k_2}$ results from $t^{L_1L_2}_{dd,\,mn}$, $t^{L_1L_2}_{da,\,mn}$, et al., Thus, the interlayer transfer induces various types of interband transitions. In the following discussion, we simply put

$$t^{L_1L_2}_{ij,\,k_1k_2}=t_z\delta_{ij}\delta_{k1k_2} \tag{3.4}$$

where it is assumed that the $2D$ momentum (parallel to the layer) of a hole is conserved in the interlayer hopping processes.

In such a simplified treatment, $D_2(E)$ can be expressed as

$$D_2(E)=\sum_{k_z}\sum_{k_x,\,k_y}\delta(E-B_2(k)-t_z\cos k_z) \tag{3.5}$$

where k_z specifies the momentum in the direction perpendicular to the layers. Putting $z=\cos k_z$, we have

$$\begin{aligned} D_2(E)&=(2\pi)^{-1}(\pi/2)^{-2}\int_{-1}^{1}dz(1-z^2)^{-1/2}\,|\,\overline{E}-t_zz-E_a\,|^{-1}\\ &\times\int_0^1 dz[x(1-x)]^{-1/2}[h(x,\,\overline{E}-t_zz)\,(1-h(x,\,\overline{E}-t_zz))]^{-1/2}\\ &\times\theta(h(x,\,\overline{E}-t_zz))\theta(1-h(x,\,\overline{E}-t_zz))\,|\,3[E_2(x,\,h(x,\,\overline{E}-t_zz))]^2\\ &-2(E_d+E_a+E_b)\,E_2(x,\,h(x,\,\overline{E}-t_zz))+E_aE_b+E_bE_d+E_dE_a\\ &-t_a{}^2x-t_b{}^2h(x,\,\overline{E}-t_zz)\,| \end{aligned} \tag{3.6}$$

From the above relation, we find that $D_2(E)$ is nonzere in the energy range, $E_a-t_z\leqq\overline{E}\leqq E_b+t_z$. To investigate the behavior of $D_2(E)$ near the band edge, $\overline{E}=E-t_z$, we put

$$E=E_a-t_z+t_zp,\ \ (\overline{E}=E-E_{2,\,c}) \tag{3.7}$$

with $0<p<<1$. Then, we have

$$\begin{aligned} D_2(E)&\propto(E_b-E_a)^{-1}\int_{-1}^{-1-p}dz(1-z^2)^{-1/2}\\ &\times\int_{u1(z,\,p)}^{u_2(z,\,p)}dx]x(1-x)]^{-1/2}[(x-u_1(x,\,p))(u_2(z,\,p)-x)]^{-1/2} \end{aligned} \tag{3.8}$$

where

$$u_1(z,\,p)=-t_z(E_a-E_d)\,(z+1-p)/t_a{}^2 \tag{3.9a}$$

$$u_2(z, p) = -t_z(E_a - E_d + t_b^2/(E_b - E_a))(z+1-p)/t_a^2 \qquad (3.10)$$

From (3.8), it follows that

$$D_2(E) \propto (E_b - E_a)^{-1} \int_{-1}^{-1+p} dz[-t_z(1-z^2)(z+1-p)]^{-1} \times F[\pi/2, 1+(E_a-E_d)(E_b-E_a)/t_b^2] \qquad (3.11)$$

with the function F defined by the elliptic function,

$$F[\pi/2, k] = \int_0^{\pi/2} dx(1-k^2\sin^2 x)^{-1/2} \qquad (3.12)$$

It is easy to confirm that F satisfies the relation,

$$\lim_{k\to 1} F[\pi/2, k] \to 1/2 \log(1-k^2) \qquad (3.13)$$

Then, for $E_a \fallingdotseq E_d$ or $E_a \fallingdotseq E_b$, we have

$$D_2(E) \propto (E_b - E_a)^{-1} |\log(E_a - E_d)(E_b - E_a)| \qquad (3.14)$$

Noting that

$$\int_{-1}^{-1+p} dz[(z+1)(-1+p-z)]^{-1/2} = \pi \qquad (3.15)$$

we find from (3.11) that $D_2(E)$ takes a finite value at the limit $p \to 0$. Similar discussion can be applied to the upper band edge, $\bar{E} = E_b + t_z$. Thus, we find that the $E^{-1/2}$-singularity at the band edges of the E_2-band vanishes in the presence of the small interlayer transfer, although the peak structure is almost unchanged, as shown by the dotted curves in Fig. 3.

§ 4. The influence of the singularity-enhanced density of states on the tunneling current and the isotope effect

In this section, we first investigate how the singularity-enhanced density of states discussed above affects on the behavio of the tunneling current, which can flow between the two superconductors separated by a thin dielectric barrier. Tunneling spectroscopy is one of the powerful methods to clarify the nature of the superconductors.

From a Hamiltonian formalism of the tunneling problem, the tnnneling current can be expressed as

$$I(t, V) = I_{qp}(V) + I_J(V)\sin F(t) + \cdots \qquad (4.1)$$

where $F(t) = \text{cons.} + 2eVt/h$ with the time index t and the static

bias voltage V. I_{qp} is the quasi-particle current, I_J is the Cooper pair's phase coherent tunneling transition, and the dots stand for the other tunneling components such as the quasi-particle-Cooper pair interference component. In the following, we calculate the V-dependences of I_{qp} and I_J, which in the framework of BCS theory are defined as[11]

$$I_{qp}(V)=h/eR_N\int_{-\infty}^{+\infty}dE\ n_L(E)n_R(E-E_0)\,[f(E-E_0)-f(E)] \tag{4.2}$$

$$I_J(V)=(h/\pi eR_N)P\int_{-\infty}^{+\infty}dE\int_{-\infty}^{+\infty}dE'\frac{p_L(E)\,p_R(E')}{E-E'-E_0}\times[f(E)-f(E')] \tag{4.3}$$

where $E_0=eV/h$, $R_N=h^3/4\pi e^2t^2$ with the averaged transfer integral t, and P in (4.3) means taking the principle value. n_i and p_i $(i=L,R)$ are given by

$$n_i(E)=|E|D(E^2-|A_i|^2)^{-1/2}\theta(|E|-|A_i|) \tag{4.4}$$

$$p_i(E)=|A_i|D(E^2-|A_i|^2)^{-1/2}\mathrm{sgn}(E)\theta(|E|-|A_i|) \tag{4.5}$$

with the order parameter A_i and

$$f(E)=[\exp(E/k_BT)+1]^{-1} \tag{4.6}$$

In the above formula, we note the energy E-dependence of the density of states D. This dependence is particularly important when the Fermi energy is located near the singular of D. In numerical computations, we confine ourselves to the case of the low E_2-hole concentration; the Fermi energy is near the bottom of the E_2-band, and thus near the $E^{-2/2}$-singularity. Then, the low-voltage behavior of the tunneling current is dominated by this singularity, while the contribution of the E_1-band is similar to the flat band case. In such a situation, replacement of D in (4.2) and (4.3) qy D_2 is considered to be reasonable. We also assume that the order parameter of the left and right superconductors are equal to each other, i.e. $A_L=A_R=A$.

The numerical results for the V-dependence of I_{qp} at $T=0$ are illustrated in Fig. 5, where $E_0=eV/2A$ and $\tilde{I}_{qp}=(eR^N/h)I_{qp}$. At

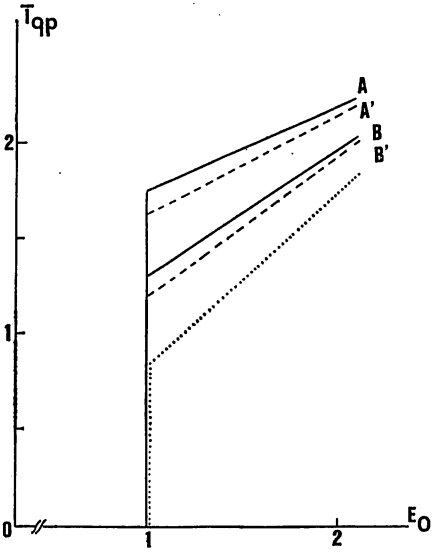

Fig. 5. The contribution of D_2 to the quasi-particle tunneling current, I_{qp}, defined by (4.2). $\bar{I}_{qp}=(eR_N/2A)I_{qp}$ and $E_0=eV/2A$. The solid curves A and B correspond to $\tilde{E}_F=5A$ and $10A$, respectively, with $W_2=200A$. The dashed curves A' and B' represent the modifications of A and B due to the ihterlayes transfer ($t_z=10^{-2}t_a$). The parameter values are the same as those empleyed in Fig. 3. The dotted curve gives I_{qp} for the flat E_2-band, i.e. $D_2(E)=1/W_2$.

$T=0$, I_{qp} vanishes for $E_0<1$, whereas for $E_0>1$ I_{qp} increases with increasing E_0. The solid curves A and B correspond to $\tilde{E}_F=5A$ and $10A$, respectively, where $\tilde{E}_F$ is the Fermi energy measured from the bottom of the E_2-band. In these calculations, we have put $W_2=200A$ with W_2 being the E_2-bandwidth. The dashed curves A' and B' represent the modifications of the curves A and B due to the small but non-vanishing interlayer transfer t_z defined by (3.4) (In Fig. 5, $t_z=10^{-2}t_a$). The dotted curve gives I_{qp} in the flat band case, i.e. $D_2=1/W_2$. Comparison of the solid and dotted curves indicates that the singularity at the bottom of the E_2-band

enhances significantly the quasi-particle current in the situation we are considering. Although the interlayer tunsfer t_z tends to suppress the enhancement of I_{qp}' through the redudtion of the singular behavior of D_2' the appreciable enhancement of I_{qp} is still observed for t_z of the order $10^{-2}t_a$. Comparing the solid curves with the dotted curve, we also find that the $E^{-1/2}$-singularity at the bottom of the E_2-band tends to surpress the value of the derivative of I_{qp} with respect to the bias voltage V. For example, we $I_a'(V)/I_0'(V)=0.4$ and $I_b'(V)/I_0'(V)=0.5$, where I_a' and J_b' are $dI_{qp}(V)/dV$ for the solid curves A and B, and I_0' for the dotted curve in Fig. 5. Such a trend is resulted from the fact that for the position of the Fermi energy under consideration, the unoccupied density of states, D_2' decreases rapidly with incresing B (owing to the $E^{-1/2}$-dependence of D_2). In Fig. 6, we present the results for the Cooper pair's phase coherent current I_J. The solid curves A and B correspond to $\tilde{E}_F=5A$ and $10A$, respectively, and the dotted curve represents the result for the flat band case, i.e. $D_2=1/W_2$. Similarly to the calculation of I_{qp}' we have put $W_2=200A$. In the variation of I_J with E_0' one of the characteristic features is the occurence of the Riedel peak at $E_0=1$.[12] This peak is due to the singular behavior of the superconducting density of states at $E=A$. The gross features of I_J are common to the three cases (the solid curves A and B and the dotted curve). However, for a given E_0' the singularity-enhanced density of states leads to the appreciable enhancement of I, similarly to the case of I_{qp}.

Our next task is to investigate the influence of the singularity-enhanced density of states on the isotope effect. The BCS gap equation is given by

$$A(k_1)=-\sum_{k_2}V_{k1k_2}\frac{A(k_2)}{2\tilde{E}(k_2)}\tan h[\tilde{E}(k_2)/2k_BT] \qquad (4.7)$$

where $\tilde{E}(k)=[(E(k)-E_F)^2+A(k)^2]^{1/2}$ with the single-particle energy $E(k)$ and the Fermi energy E_F. The critical temperature

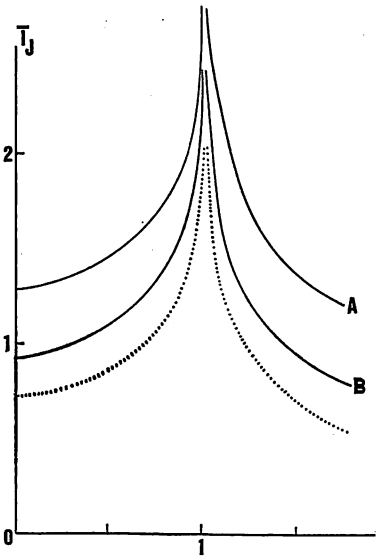

Fig. 6. The contribution of the E_2-band to the Cooper pair's phase cohercent current $I_{J'}$ defined by (4.3). $\bar{I}_J=(eR_N/2A)I_J$ and $E_9=eV/2A$. The parameter values for the solid curves A and B are the same as those employed in Fig. 5. The dotted curve corresponds to the flat E_2-kand case, i.e. $D_2(E)=1\cdot W_2$.

T_C can be determined from the condition that (4.7) has a non-trival solution in the limit $A \to 0$. We assume that the attractive pairing interaction is approximated by the s-wave potential, i.e. $V_{k_1k_2}=-V$ for $-E_D<E_1(k)$, $E_2(k)<E_D$ and $V_{k_1k_2}=0$ for otherwise, where E_D is the Debye cutoff energy. Then, for the momentum-independent energy gap A we have the following well-known formula,

$$V^{-1}=\int_{-E_D}^{E_D} dE \frac{D(E)}{2|E-E_F|} \tan h[|E-E_F|/2k_BT_C] \qquad (4.8)$$

where $D(E)$ represents the density of states. Since we are interested in the singular behavior of D, it is inadequate for our purpose to replace D by a flat density of states. The E_D-depen-

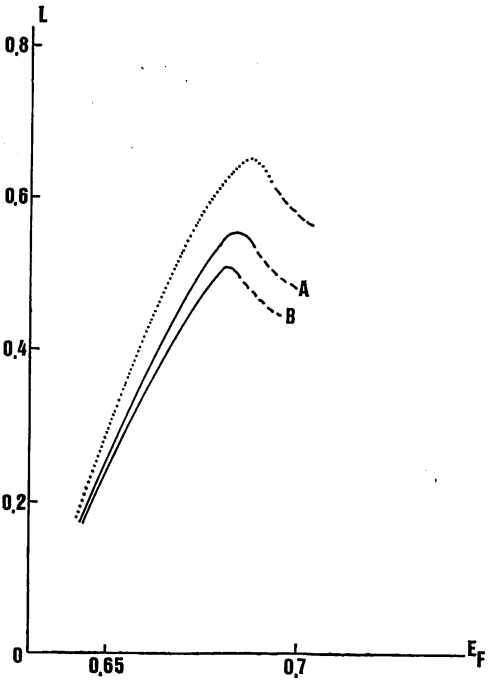

Fig. 7. The variation of L (defided by (4.9)) with the Fermi energy. The solid curve A represents the contrribution of the E_2-band (the parameter values are the as those employed in Fig. 3), and the curve B gives the modification of A due to the interlayer transfer ($t_z=10^{-2}t$). The dotted curve represents the simultaneous contributions of the E_1- and E_2-bands, for the vanishing $\triangle E$ (defined in Fig. 4)

denbe of T_C can be approximately written as

$$T_C=\text{const.}\times E_D^{1-L} \tag{4.9}$$

with an adequately chosen value of L. The above relation is equivalent to

$$L=1-\partial \log T_C/\partial \log E_D \tag{4.10}$$

In a phonon-mediated pairing mechanism, E_D is proportional to $M^{-1/2}$, where M is the average mass of the constituent atoms. Thus, L represents the deviation of the isotope effect from the

ideal case ($L=0$). The calculated variation of L with the Fermi energy is illustrated in Fig. 7, where we have put $E=4\times10^{-2}t_a$ ($t_a=t_b$) and $W_2=0.2t_a$. The solid curve A represents the contribution of the E_2-band and the curve B the modification of the curve A due to the interlayer transfer ($t_z=10^{-2}t_a$). Both curves indicate that the sharp peak structure at the bottom of the E_2-band cotribute to enhance the value of L, i.e. the suppression of the isotope effect. In the O-hole dominant model, we have seen that when the Fermi energy is located near the upper edge of the lower subband (Fig. 3), the maximum of L is estimated to be $L_{\max}\sim0.75$. In the present model, the contribution of the E_2-band leads to $L_{\max}\sim0.6$, which is smaller than that in the O-hole dominant model. Such a difference comes from the difference of the shape of the density of states between the two models. In 0 2, we have pointed out that for a set of adequate parameter values, the logarithmic van Hove singularity in the E_1-band comes very closely to the singularity at the bottom of the E_2-band, When the distance between the two singularities is of the order of E_D, the simultaneous contributions of these singularities are exdected. The dotted curve in Fig. 7 represents the result for $D=D_1+D_2$ with the above two singularities located at the same point. In this special case we have $L_{\max}\sim0.7$, which is comparable with that in the O-hole dominant model.

§ 5. Concluding remarks

In this paper, we have investigated the hole states in the *Cu*- and *O*-hole mixing model showing the asymmetry with respect to the x- and y-directions. By explicit treatment of the *Cu*-holes, some informations about the mixing effect of the *Cu*- and *O*-holes have been obtained, the informations which cannot be derived in the *O*-hole dominant model employed in the preceding paper (I).

As shown in the above discussion, the mixing of the *Cu*- and

O-hole states gives different types of singularities and different shnpe of the density of states from those in the *O*-hole dominant model. In the *Cu*- and *O*-hole mixing model, the bond asymmetry leads to the splitting of the hole band into three subbands ($E_1<E_2<E_3$). We have considered the case where the E_1-band is half-filled. Then the strong Coulomb repulsion at *Cu*-sites induces a large energy gap between the occupied and unoccupied E_1-levels. For the sufficiently large gap, the additional holes are captured by the $E^{-1/2}$-singularity at the bottom of the E_2-band, even when their concentration is extremely low. On the other hand, in the *O*-hole dominant model the bond asymmetry leads to the splitting of the *O*-band into the two subban ds;ni order to realize the Fermi energy close to the band edge singularity, comparatively high codcentration of the *O*-holes is required ($n_c\sim0.5$).

In the *Cu*- and *O*-hole mixing model, we have discussed how the tunneling current (between the two superconductors separated by a thin dielectric) is modified by the singularity enhanced density of states. Numerical computations have been done for two types of the tunneling currents, namely, the quasi-particle current I_{qp} and the Cooper pair's phase coherent current I_J. When the Fermi energy is located near the bottom of the E_2-band, the appreciable enhancement of I_{qp} is derived. However, our calculation also indicates that derivative of I_{qp} with respect to the applied voltage is rather suppressed by the singular behavior of the density of states, D_2. This is due to the rapid decreasing of the unoccupied part of $D_2(E)$ with increasing E. The Cooper pair's current I_J shows a characteristic peak structure in the variation with the applied voltage. From numerical analysis, we find that the gross feature of such a peak structure is not so strongly affected by the singularity of D_2, although the value of I_J itself is enhanced singularity.

We also have discussed the isotope effect modified by the

singularity of the E_2-band. The deviation of the isotope effect from the ideal case is given by L (defined by (4.9)). The conspicuous enhancement of L is derived for the Fermi energy located near the bottom of the E_2-band; the contribution of the E_2-band leads to the maximum value of L, $L_{max}\sim 0.6$, This value is smaller than that in the O-hole dominant model ($L_{mxa}\sim 0.75$). As described in the preceding sections, such a difference of the L_{max}-value is resulted from the difference of the state density-shape between the two models. For a set of adequate paramter values, there is a possibility that the logarithmic van Hove singularity in the E_1-band comes very closely to the bottom of the E_2-band. In such a special case, the simultaneous contributions of the singularities in the E_1- and E_2-bands leads to $L_{max}\sim$ 0.7, which is comparable with the result of the O-hole dominant model.

The E_2-band discussed above shows the conspicuous mass anisotropy. For the parameter values employed in calculating the solid curves in Fig. 5, the mass anisotropy of the E_2-holes near the Fermi surface is about m_y/m_x 2–2.5. which is larger than that estimated from the distorted vortex lattice (mentioned in § 1). For the same parameter values, the mass anisotropy of the E_2-band is about m_y/m_x 1.05–1.1. Thus, averaging of the effective mass over the E_1- and E_2-bands may tends to lead more reasonable values of the mass anisotropy. As described above, one of the characteristic features is the two dimensional property of the supercurrent, the property that induces interesting behaviors of the photon-mediated interaction between localized moments-[13)–18)] The detailed discussion will be discussed in a separate paper.

References

1) P. W. Andrson, Science, *235*, (1987), 1196.
G. Baskaran, Z. Zou, and P. W. Anderson, Solid State Commun., *13*,

(1987) 973.

2) C. M. Varma, S. Schmit-Rink, and E. Abrahams, Solid State Commun. *62*, (1987), 681.

3) V. J. Emery, Phys. Rev. Lett., *58*, (1987), 2794.

4) P. Prelovseb, T. M. Rice, and F. C. Zhang, J. Phys. C, *20*, (197) *L*229.

5) D. J. Scalapino, E. Loh, and J. Hirsh, Phys. Rev. B., *34*, (196), 8190.

6) Y. Ueda and K. Kosuge, Physica, *C156* (1988) 281.

7) D. C. Mattis and M. P. Mattis, *Theories of High T_C Superconductivity*, ed, by J. Woods Halley, Addison Wesley Publishing Company, Inc. (1988).

8) S. Seki, Prog. Theor. Phys. *83*, (1990) 455,

9) G. J. Dolan, F. Holtzberg, C. Feild and T. R. Dinger, Phys. Lett. *62*, Lett. *62*, (1989) 1184.

10) L. Ya. Vinnikov, I. V. Grigorieva, L. A. Gurevich, Yu. A. Ossipyan, in *High Temperature Superconductivity from Russia*, A. I. Larkin and N. V. Zavaritsky, eds., World Scientific, (1989).

11) Fo. example, A. Barone and G. Paterno, *Physics and Aqplications of the Josephson Effect*, John Willey & Sons, Inc., New York. (1982).

12) E. Riedel, Z. Naturforsch. *19A*, (1964) 1634.

13) S. Seki, Prog. Theor. Phys. *75*, (1986), 15.

14) S. Seki, Prog. Theor. Phys. *75*, (1986), 529.

15) S. Seki, Prog. Theor. Phys. *81*, (1989), 603.

16) S. Seki, Prog. Theor. Phys. *81*, (1989), 1174.

17) S. Seki, Solid State Communications (London), *66*, (1988), 1163.

18) S. Seki, Solid State Communications (London), *68*, (1988), 97.